Vol. 23 • No. 1 • January 4 • 2011

D10488

www.advmat.de

ADVANCED MATERIALS

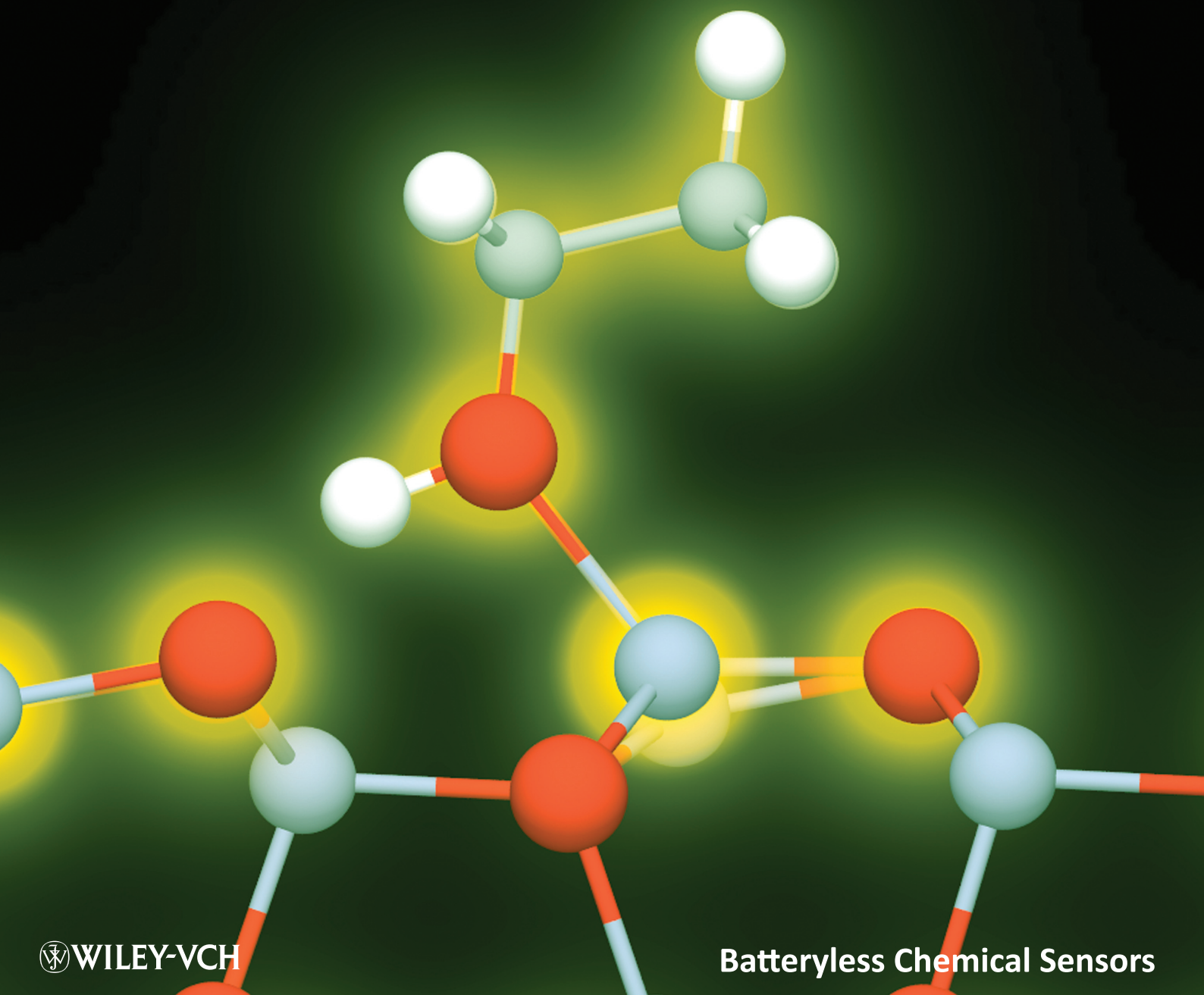

WILEY-VCH

Batteryless Chemical Sensors

ADVANCED MATERIALS
www.advmat.de

Batteryless Chemical Detection with Semiconductor Nanowires

Xianying Wang, Yinmin Wang, Daniel Åberg, Paul Erhart, Nipun Misra, Aleksandr Noy, Alex V. Hamza, and Junhe Yang*

Batteryless chemical or biological detection, i.e., sensing without the need for an external power source, is an attractive scheme that will have instant advantages over the existent sensing technology in which the gas, chemical, or biological detection is based on equilibrium thermodynamic quantities such as resistivity/conductance or capacitance that have to be monitored electrically or optically.[1–12] Semiconducting nanowire- or nanotube-based sensors have been well-documented to exhibit an ultrasensitive detection limit because of their large surface-to-volume ratio. Despite their relatively small power consumption (as little as sub-microwatts power),[1,4,8,13] these sensing platforms (or any other existing solid-state bulk sensors) require an external power source (battery) to operate. This, to large extent, curbs the nanosensor sizes and their reachable locations, as the macroscopic dimensions of power sources often far exceed those of nanosensors. It has been proposed that the small power needed for such a nanosensor can be harvested from the surrounding environment.[14] For this purpose, however, specific types of environmental energy sources have to exist. In addition, the fabrication of such an energy nanogenerator is highly non-trivial, and in most cases, prohibitively expensive and bulky to be integrated into nanosensor systems.[15–17]

In this Communication, we report the fabrication of the first generation batteryless sensors that use one-dimensional semiconductor nanowires. These nanosensors take advantage of a unique interaction mechanism between chemical species and semiconductor nanowire surfaces that induce an electric potential between the two ends of nanowires or between the exposed and unexposed nanowires. As a prototype study, we demonstrate the sensing ability of our batteryless sensors with two different types of platforms, using ethanol solvent as a testing agent.

Figure 1a and b show schematically the designs of two different sensing platforms, respectively. The first platform, Figure 1a, is fabricated from the vertically-aligned single-crystalline ZnO nanowires (n-type), and the second one, Figure 1b, utilizes randomly-aligned boron-doped silicon nanowires (p-type). We choose ZnO and Si nanowires as they have been proved to be good sensor materials.[1,7,8,10] In the first sensing platform, we expose the tips of nanowires to chemical species and monitor the change of the electric potential along the two ends of nanowires (Figure 1a). In the second platform, about 80% of silicon nanowire network is sealed with insulation glue, leaving the rest of nanowires exposed to chemical species. In this platform, the potential difference between the exposed and unexposed nanowires is monitored (Figure 1b).

The as-grown ZnO nanowires have a length of ~6–7 μm and an areal density of ~30/μm^2, as shown in Figure 1c. After the growth, ZnO nanowire forest was infiltrated with a poly(vinyl chloride-co-vinyl-co-2-hydroxypropyl acrylate) (PVC) polymer and etched with oxygen plasma, leaving ~0.1–0.5 μm nanowire tips exposed. Based on the nanowire density given above, the exposed surface area of the nanowires is estimated to be 6.6 μm^2 per μm^2 device area. The carrier concentration of these as-synthesized ZnO nanowires is on the order of $5.2 \pm 2.5 \times 10^{17}$ cm^{-3}, as reported in the reference.[18] For sensing experiments, Au/Ti (100 nm/4 nm) film and Ag paste were used to make the top and bottom electrical contacts, respectively. Standard electric current versus voltage (I–V) measurements (–0.5 V ~ 0.5 V) are applied to check that good electrical contacts are made.

The diameters of the Si nanowires are around 30–55 nm and the lengths are up to tens of micrometers,[19] Figure 1d. To test the sensing property of the Si nanowire interconnection network, Au(100 nm)/Ti(4 nm) film was evaporated on two opposite sides of the substrate as electrical contacts. Insulation glue was then applied to seal one side of the electrode and 80% of the silicon nanowire network. Again, standard I–V scans are adopted to ensure that good electrical contacts are made on all test-bound devices.

To probe the effectiveness of the ZnO nanosensor (i.e., platform one in Figure 1a) on chemical species at room temperature, we drip a small volume (~2.2 μL) of ethanol (≥99.5%, SIGMA-ALDRICH, St. Louis, MO, USA. ≤0.005% water) on the device surface and monitor the change of the electric voltage between the two ends of nanowires. A sharp rise of an electric voltage with the peak value on the order of ~170 mV is observed, **Figure 2a**. The rise of the electric signal is almost instantaneous but decays slowly to zero level as the ethanol solvent evaporates. This result indicates that the chemical sensor made of ZnO nanowires is recoverable. Interestingly, little electric

Dr. Y. M. Wang, Dr. D. Åberg, Dr. P. Erhart, Dr. N. Misra, Dr. A. Noy, Dr. A. V. Hamza
Nanoscale Synthesis and Characterization Lab
Lawrence Livermore National Laboratory
Livermore, CA 94550, USA
E-mail: ymwang@llnl.gov
Prof. X. Y. Wang, Prof. J. H. Yang
School of Materials Science and Engineering
University of Shanghai for Science and Technology
Shanghai 200093, China

DOI: 10.1002/adma.201003221

© 2011 WILEY-VCH Verlag GmbH & Co. KGaA, Weinheim

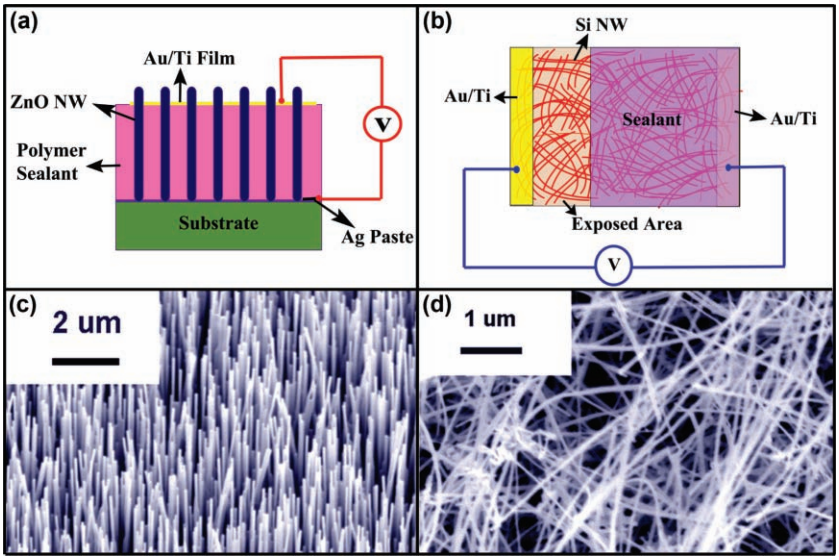

Figure 1. Schematics of chemical sensor design using (a) vertically- or (b) randomly-aligned nanowire platforms, respectively. Scanning electron micrographs of (c) as-grown ZnO nanowires, and (d) Si nanowires, respectively.

voltage is observed when a small amount of hexane solvent (≥99.0%, SIGMA-ALDRICH, St. Louis, MO, USA. ≤0.001% water) is dripped onto the surface of the same device (blue curve in Figure 2a), suggesting that the nanosensor selectively responds to different types of solvent molecules. These experiments, together with our measurements using more than 15 different types of organic solvents (e.g., hexane, acetone, benzene, chloroform, toluene, 1,4 Dioxane, 1-butonal, 1-propanol, pyridine, N,N-dimethylacetamide, and dimethyl sulfoxide ; also see **Table 1** and Supporting Information Figure S1–S4), strongly suggest that the magnitude of the peak voltage scales sensitively with the dipole moment (μ) and surface coverage of the tested solvents, with non-polar solvents such as hexane and benzene generating essentially zero electric voltage. This trait makes it possible for our nanosensors to detect different types of chemical species and their concentration levels.

It is noteworthy to point out that, unlike other types of high dipole moment molecules, interestingly, de-ionized water (μ = 1.85D) produces little voltage signal in our nanodevices (Supporting Information, Figure S4). This is likely due to the fact that the surface tension of water (71.99 nN/m) is more than three times higher than that of ethanol (21.97 nN/m), leading to poor surface wetability in our nanodevices. The negligible voltage signal observed by water eliminates the possibility of water (in the air or in some solvents) contamination/contribution to our nanosensors.[20]

To test the sensing ability of ZnO platform to small concentrations of ethanol solvent, we mix different percentages of ethanol with hexane (note that hexane does not generate voltage signal in our device) and drip them onto the surface of the nanosensor. The dripping volume is fixed at ~2.2 μL per drop. The voltage measurement results shown in Figure 2b demonstrate that the induced peak electric voltage increases stepwise with the concentrations of ethanol solvent, and that the voltage signal is reversible for decreasing or increasing ethanol concentrations. The lowest concentration level we have tested so far using ZnO nanowire platform is 0.27 vol.%, which yields a peak voltage signal of 11.7 mV. A higher detection limit is possible as our electric probe station has a voltage resolution better than one tenth of mV (~50 μV, equivalent to 10 ppm ethanol concentration level).

To establish reproducibility, we carried out three independent measurements on one single device, as displayed in the inset of Figure 2b, showing that the concentration dependence of the voltage signal is slightly non-linear. We observed this non-linearity in all five good devices we tested. There are two possible reasons that could have contributed to this behavior. First, the vertically-aligned ZnO nanowires have different exposure height (~0.1–0.5 μm), which may lead to different magnitudes of voltage signals for each individual nanowire and collectively contribute to the overall output voltage. Second, the observed nonlinear response may also suggest that the change of the electron affinity of ZnO nanowires after molecular adsorption is non-linear, as it could have a complex dependence on surface coverage, molecular size, dipole moment, and surface tension of the solvents.[21] We found that, independent of the ethanol concentration levels, the recovery time of our nanosensor is relatively short (<100 s). The fast recoverable time of our nanosensor is due to the volatile nature of ethanol and hexane in ambient atmosphere, and is advantageous over other nanowire-based sensors that, because of large surface-to-volume ratios, often have a much longer recovery time.[3,8]

Note that in both platforms (Figure 1a and b), the tested solvents also wet one metal contact of our nanodevices. It is known that the electrochemical potential of a metal contact can be shifted once immersed into liquid solutions/solvents. We have thus carried out additional experiments to quantify the accurate value of this electrochemical potential shift using devices without nanowire protrusions, as well as a device fabricated from single-crystal ZnO. In both cases when ethanol solvent was used, we observed a voltage signal on the order of ~1 mV (Supporting Information, Figure S5), consistent with the results reported by Ghosh et al. on carbon-nanotube metal interfaces,[22] and supporting our suggestion that the active functioning ingredients in our nanosensors are semiconducting nanowires rather than the metal contacts.

Figure 2c shows the electric voltage of the silicon nanowire device in response to different concentrations of ethanol solvent. A similar decreasing trend is observed in this device with the decreasing ethanol concentrations. Furthermore, we found that the decay shape of the electric voltage as a function of time is drastically different from that of ZnO nanowire sensors, possibly due to the change of the wetting area difference between ZnO and silicon nanowire devices. The irregular decay shape of the voltage signal in the silicon nanowire device is currently not well-understood and requires further investigations. Nonetheless, these results demonstrate that it is possible to extend

© 2011 WILEY-VCH Verlag GmbH & Co. KGaA, Weinheim

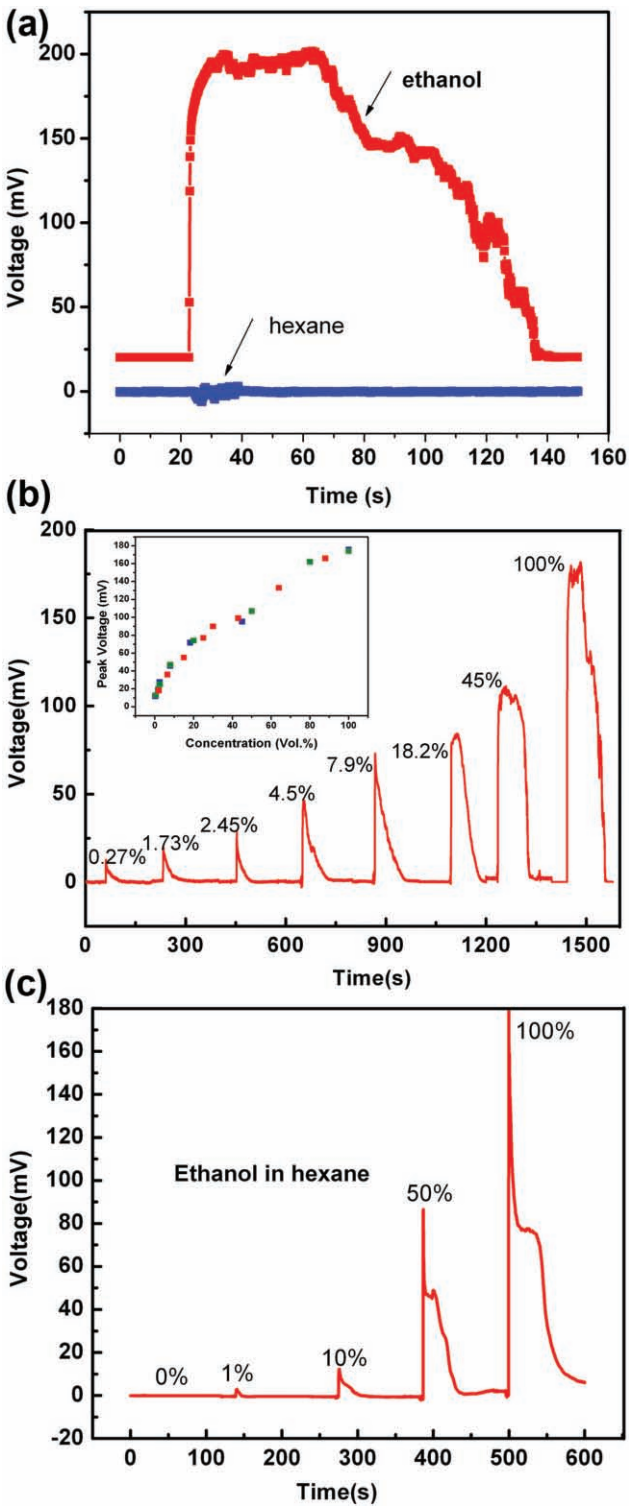

Figure 2. (a) Voltage signals of ZnO nanowire platform in response to pure ethanol and pure hexane solvent, respectively. (b) The change of voltages in ZnO nanosensor responds to different concentrations of ethanol solvent. The inset is the peak voltage signal versus ethanol concentration as obtained from three independent measurements (blue, green, red solid squares, respectively) on the same device. A slightly nonlinear behavior is observed. (c) Voltage signals of randomly-aligned Si nanowire sensors respond to different ethanol concentration levels.

Table 1. Representative chemicals tested on our nanodevices and their physical properties at 25°C.[31] The generated voltages were measured on each of five different ZnO nanowire devices in ambient atmosphere. All the solvents (except water) listed here were acquired from SIGMA-ALDRICH, St. Louis, MO, USA.

Chemical name	Linear formula	Purity	Density (g/mL)	Dipole moment (D)	Open circuit voltage measured (mV)
Ethanol	CH_3CH_2OH	≥99.95%	0.789	1.69	~130–170
Hexane	$CH_3\ (CH_2)_4CH_3$	≥99.0%	0.659	0	~0–3
Water	H_2O	≥99.9%	1.000	1.85	~0–0.3
Acetone	CH_3COCH_3	≥99.9%	0.793	2.88	~190–270
Chloroform	$CHCl_3$	≥99.8%	1.483	1.08	~28–37
Dimethyl sulfoxide	$(CH_3)_2SO$	≥99.9%	1.100	3.96	~55–65

the batteryless sensing platform to randomly-aligned semiconductor nanowire systems.

The working principle of our nanosensors relies on partial exposure of semiconducting nanowires to target chemical species and a non-ohmic contact that is necessary for the nanosensors to function. Qualitatively, the energy-band diagram of our devices is shown in **Figure 3a**. The Fermi level, conduction band, and valence band of the devices before chemical exposure are denoted as E_F, CB, and VB, respectively. Note that there exists a non-ohmic contact and band bending (upwards bending for ZnO, and downwards bending for Si) in both devices. Upon adsorption of molecules (such as ethanol), it is known that the carrier density (electrons for n-type ZnO nanowires, and holes for p-type Si nanowires) of the exposed nanowire segment is altered, leading to profile modification of CB to CB'.[1,23] This process metastably tilts the Fermi level of nanowires from E_F to E_F', and renders a detectable potential offset between the top (Au) and ground (Ag) contacts. The thermodynamic re-equilibration of the Fermi level will require electron drift/diffusion through the non-ohmic contact or through a discharge process by short-circuiting the top and ground contacts. This qualitative picture suggests that the magnitude and shape of the voltage signals we observed are closely tied to the electron donating/withdrawing ability of molecules (as well as their other physical properties), the nature of the non-ohmic contact (which can be modified by molecules), and the charge carrier density (electrons or holes) within the nanowires. In the case of an ohmic top contact or near metallic nanowires (for example, highly-doped Si nanowires), we did not see appreciable voltage signals from ethanol solvent, which is in accord with our above hypotheses.

To quantitatively understand the physical origin/mechanism of our nanosensors, we further carried out quantum mechanical calculations using density functional theory (DFT). For simplicity, the calculations focus on the chemisorption effects (using ethanol molecule as a prototype) on the electron affinity (χ) and work function (ϕ) of semiconducting ZnO nanowires. The results indicate that ethanol molecule has a negative adsorption energy when it interacts with ZnO nanowire top ((0001) or $(000\bar{1})$) or side $(10\bar{1}0)$ surfaces. This negative

© 2011 WILEY-VCH Verlag GmbH & Co. KGaA, Weinheim

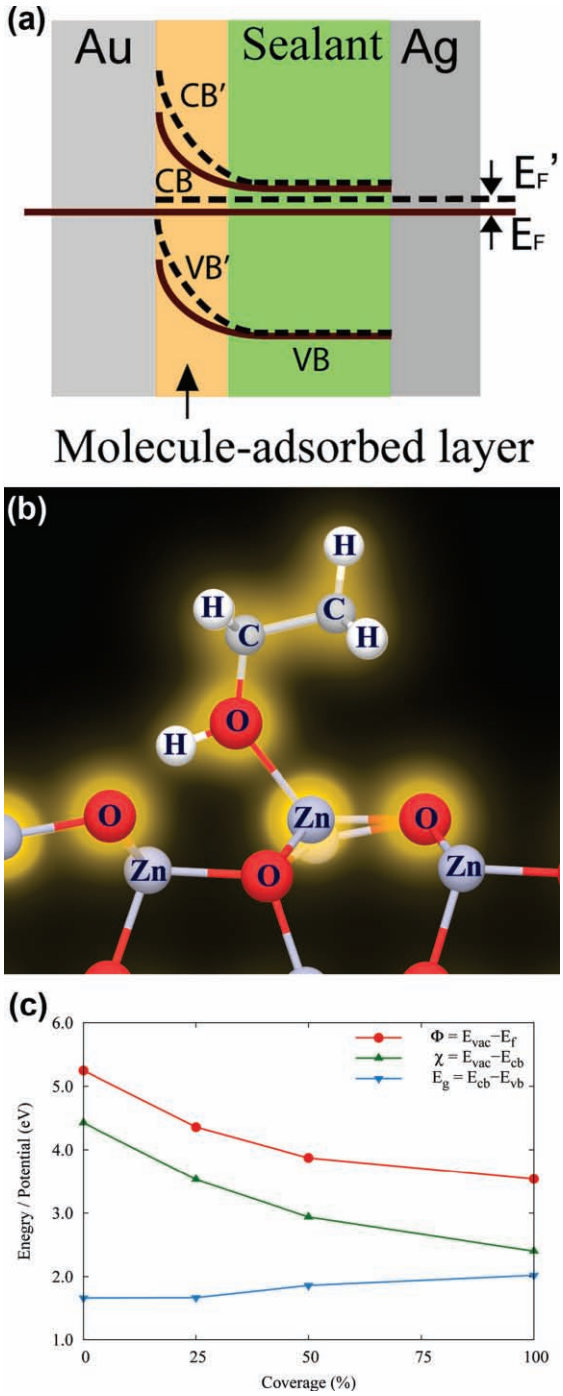

Figure 3. (a) Schematic energy-band diagram of the nanosensor before and after molecular adsorption. (b) The minimum energy configuration of ethanol structure after adsorption on the side surface of ZnO nanowires, indicating that the adsorption of ethanol on ZnO surface is characterized by the formation of a chemical bond between the O-atom in ethanol and a Zn-atom, and a hydrogen bridge bond between ethanol and an O-atom in ZnO. The yellow color in the figure represents the electron density. Note the slight overlapping of the yellow color between an H-atom and an O-atom in ZnO. (c) The change of work function (ϕ), electron affinity (χ), and band gap (E_g) of ZnO surface as a result of the adsorption of ethanol molecules onto the side surface, as obtained from quantum mechanical calculations. The surface coverage in the figure is defined as the ratio of molecule numbers over ZnO unit cells.

adsorption energy is the main driving force that allows ethanol molecules to be adsorbed. Figure 3b indicates that under the minimum energy configuration condition, the adsorption of ethanol onto ZnO surfaces is characterized by the formation of a chemical bond between the O-atom in ethanol and a Zn-atom, as well as a hydrogen bridge bond between an H-atom and an O-atom in ZnO. After adsorption, we found that the electron affinity, as well as the work function, of ZnO nanowires in contact with ethanol molecules has been substantially altered, as shown in Figure 3c. The change of the electron affinity scales approximately with the surface coverage, but shows a non-linear behavior that qualitatively agrees with our experimental observations. Under the minimum energy interaction configurations, Figure 3c indicates that the absolute value of electron affinity (χ) of clean ZnO surface decreases from 4.5 eV to 2.4 eV when the surface coverage of ethanol increases from 0 to 100%, whereas the band gap remains fairly constant. We note that the electron affinity changes from our calculations are about one order of magnitude higher than those we measured from experiments, possibly due to the reasons that (1) the calculations used clean ZnO surfaces such that their interactions with molecules are stronger, and (2) the change of the electron affinity may not completely reflect on the measured potentials, as the thermodynamic re-equilibration process tends to reduce the potentials. Nonetheless, the change of the electron affinity of ZnO when exposed to ethanol solvents is consistent with the qualitative picture depicted in Figure 3a and appears to be the main reason that leads to the large electric potential difference between the two contacts of ZnO nanowires. In addition to the surface coverage, our calculations also revealed that the dipole moment of the solvent molecules and its orientations relative to the ZnO surfaces have direct impacts on the magnitude of the electron affinity change. Since different organic molecules have different dipole moments, this characteristic makes our nanosensors promising to detect different types of chemical- or bio-molecules.

In summary, we have demonstrated two different types of batteryless sensing platforms at room temperature using either vertically-aligned ZnO or randomly-aligned silicon nanowires. Unlike traditional chemical or biological sensors, the sensing platforms we described here rely on the changes of charge carriers that induce electric potentials along nanowires or between different nanowires when exposed to chemical species. Since our nanosensors do not hinge on equilibrium thermodynamic variables,[24] they have fast response time (better than 1s), relatively high sensitivity, and more importantly, do not require external power sources. As such, the power-consumption of our nanosensors is no longer a major concern. Since most organic molecules in living systems have a tangible dipole moment, it is expected that the chemical sensor reported here is also applicable to biological systems.

Experimental and Modeling

The vertically aligned ZnO nanowires with diameters in the range of 60–120 nm were grown on an a-plane sapphire substrate using a chemical vapor transport and condensation (CVTC) process.[18] The growth temperature and time are 915–930 °C and 3–5 min, respectively. After growth, the ZnO nanowire forest was filled with poly(vinyl chlori

© 2011 WILEY-VCH Verlag GmbH & Co. KGaA, Weinheim

de-co-vinyl-co-2-hydroxypropyl acrylate) (PVC), which is cured at room temperature for 24 hours. An oxygen plasma etching process was employed to preferentially etch away the PVC and expose the NW tips. This process was carried out on a reactive ion etching system with an operation power of 300 W and an oxygen flow rate of 90 standard cubic centimeters per minute (sccm). The etching time is 3–5 min. The top metal contact of ZnO nanosensor was deposited by e-beam evaporation, and the bottom contact was prepared by applying the silver paste.

Randomly-aligned Si nanowires were fabricated using a vapor-liquid-solid (VLS) process.[25] The Si nanowires were grown on 2 mm × 4 mm <111>Si substrate covered with 250 nm native oxide layer.[26] Gold nanoparticles (Ted Pella, Inc.) with an average diameter of 30 nm were used as the catalyst. SiH_4 (Voltaix, Inc.) was used as the precursor and B_2H_6 (Voltaix, Inc.) as a dopant. The ratio of SiH_4 to B_2H_6 was set to 4000:1. The nanowires were grown at 420–460°C for 30 min. Both contacts of the Si nanowire device were prepared by e-beam evaporation. All the electrical measurements were carried out using a Keithley 2602 System Source Meter with a custom-built Labview controlling program.

To model the interactions between the ethanol and the clean ZnO surface, we have carried out quantum mechanical calculations within the framework of density functional theory in the generalized gradient approximation (GGA) using the Vienna ab-initio simulation package.[27,28] The atomic cores were replaced by pseudopotentials in the projector augmented wave formalism, and the Zn-3d electrons were treated as valence electrons. As the band gap of ZnO is treated poorly by the GGA, we also applied the GGA+U method by Dudarev et al.[29] with U-J = 7 eV. The occupation numbers where determined using a Gaussian smearing of 0.1 eV. For the bulk this yielded the lattice parameters $a = 3.196$ Å and $c = 5.132$ Å, together with the internal parameter $u = 0.381$. Slab models were created from 16 atomic and 16 vacuum layers along the $[10\bar{1}0]$ direction. For these systems the Brillouin zone was sampled using a $2 \times 2 \times 1$ Monkhorst-Pack[30] mesh for a cell with 2×2 cross section. Structures were converged until the forces were below 30 meV/Å.

Supporting Information

Supporting Information is available from the Wiley Online Library or from the author.

Acknowledgements

The authors have filed U.S. patent applications (61/253890, 61/255571, 61/286858) related to this research. Y.M.W and A.N are partially supported by the Defense Threat Reduction Agency-Joint Science and Technology Office for Chemical and Biological Defense (Grant no. BRBAA07-F-1–0066). The work at USST is supported by China 973 Program (2010CB234609), Shanghai NanoProject (1052nm03000), NSFC (51072119), Shanghai Rising Star Program (09QA1404100). The authors would like to thank Dr. L.Y. Woo for her assistance in sensing experiments, Prof. D.J. Sirbuly for his early contributions to this project, and Dr. S.O. Kucheyev for providing single crystal ZnO bulk samples. This work was performed under the auspices of the U.S. Department of Energy by Lawrence Livermore National Laboratory under Contract DE-AC52–07NA27344.

Received: September 4, 2010
Published online: November 30, 2010

[1] Y. Cui, Q. Q. Wei, H. K. Park, C. M. Lieber, *Science* **2001**, *293*, 1289.
[2] D. J. Sirbuly, N. O. Fischer, S. C. J. Huang, A. B. Artyukhin, J. B. H. Tok, O. Bakajin, A. Noy, *ACS Nano* **2008**, *2*, 255.
[3] J. Kong, N. R. Franklin, C. W. Zhou, M. G. Chapline, S. Peng, K. J. Cho, H. J. Dai, *Science* **2000**, *287*, 622.
[4] Y. L. Wang, X. C. Jiang, Y. N. Xia, *J. Am. Chem. Soc.* **2003**, *125*, 16176.
[5] E. S. Snow, F. K. Perkins, E. J. Houser, S. C. Badescu, T. L. Reinecke, *Science* **2005**, *307*, 1942.
[6] L. C. Tien, P. W. Sadik, D. P. Norton, L. F. Voss, S. J. Pearton, H. T. Wang, B. S. Kang, F. Ren, J. Jun, J. Lin, *Appl. Phys. Lett.* **2005**, *87*, 222106.
[7] H. T. Wang, B. S. Kang, F. Ren, L. C. Tien, P. W. Sadik, D. P. Norton, S. J. Pearton, J. Lin, *Appl. Phys. Lett.* **2005**, *86*, 243503.
[8] E. Comini, G. Faglia, G. Sberveglieri, Z. W. Pan, Z. L. Wang, *Appl. Phys. Lett.* **2002**, *81*, 1869.
[9] S. Choopun, N. Hongsith, P. Mangkorntong, N. Mangkorntong, Phys. *E-Low Dimen. Sys. Nano.* **2007**, *39*, 53.
[10] T. J. Hsueh, S. J. Chang, C. L. Hsu, Y. R. Lin, I. C. Chen, *Appl. Phys. Lett.* **2007**, *91*, 053111.
[11] S. O. Kucheyev, J. Biener, Y. M. Wang, T. F. Baumann, K. J. Wu, T. van Buuren, A. V. Hamza, J. H. Satcher, J. W. Elam, M. J. Pellin, *Appl. Phys. Lett.* **2005**, *86*, 083108.
[12] P. H. Yeh, Z. Li, Z. L. Wang, *Adv. Mater.* **2009**, *21*, 4975.
[13] Y. Huang, X. F. Duan, Y. Cui, L. J. Lauhon, K. H. Kim, C. M. Lieber, *Science* **2001**, *294*, 1313.
[14] S. Xu, Y. Qin, C. Xu, Y. G. Wei, R. S. Yang, Z. L. Wang, *Nat. Nanotechnol.* **2010**, *5*, 366.
[15] B. Z. Tian, X. L. Zheng, T. J. Kempa, Y. Fang, N. F. Yu, G. H. Yu, J. L. Huang, C. M. Lieber, *Nature* **2007**, *449*, 885.
[16] X. D. Wang, J. H. Song, J. Liu, Z. L. Wang, *Science* **2007**, *316*, 102.
[17] M. Alexe, S. Senz, M. A. Schubert, D. Hesse, U. Gosele, *Adv. Mater.* **2008**, *20*, 4021.
[18] J. Goldberger, D. J. Sirbuly, M. Law, P. Yang, *J. Phys. Chem. B* **2005**, *109*, 9.
[19] N. Misra, J. A. Martinez, S. C. J. Huang, Y. M. Wang, P. Stroeve, C. P. Grigoropoulos, A. Noy, *Proc. Natl. Acad. Sci. USA* **2009**, *106*, 13780.
[20] S. Al-Hilli, M. Willander, *Sensors* **2009**, *9*, 7445.
[21] Y. Selzer, D. Cahen, *Adv. Mater.* **2001**, *13*, 508.
[22] S. Ghosh, A. K. Sood, N. Kumar, *Science* **2003**, *299*, 1042.
[23] A. Sadrzadeh, A. A. Farajian, B. I. Yakobson, *Appl. Phys. Lett.* **2008**, *92*, 022103.
[24] B. Gergen, H. Nienhaus, W. H. Weinberg, E. W. McFarland, *Science* **2001**, *294*, 2521.
[25] Y. Cui, L. J. Lauhon, M. S. Gudiksen, J. F. Wang, C. M. Lieber, *Appl. Phys. Lett.* **2001**, *78*, 2214.
[26] J. A. Martinez, N. Misra, Y. M. Wang, P. Stroeve, C. P. Grigoropoulos, A. Noy, *Nano Lett.* **2009**, *9*, 1121.
[27] G. Kresse, J. Hafner, *Phys. Rev. B* **1993**, *47*, 558.
[28] G. Kresse, J. Furthmuller, *Phys. Rev. B* **1996**, *54*, 11169.
[29] S. L. Dudarev, G. A. Botton, S. Y. Savrasov, C. J. Humphreys, A. P. Sutton, *Phys. Rev. B* **1998**, *57*, 1505.
[30] H. J. Monkhorst, J. D. Pack, *Phys. Rev. B* **1976**, *13*, 5188.
[31] D. R. Lide, *CRC Handbook of Chemistry and Physics*, CRC Press/Taylor and Francis, Boca Raton, FL **2007**.

© 2011 WILEY-VCH Verlag GmbH & Co. KGaA, Weinheim